Desalination and Water Treatment
www.deswater.com
doi: 10.5004/dwt.2022.28924

274 (2022) 219–229
October

Effect of surface roughness on mixed salt crystallization fouling in pool boiling

Morgan Messer[a], Kyle Anderson[a], Xiang Zhang[b], Bahman Abbasi[a,*]

[a]*Oregon State University, 1500 SW Jefferson Way, Corvallis, OR 97331, USA, emails: AbbasiB@oregonstate.edu (B. Abbasi), messerm@oregonstate.edu (M. Messer), andersky@oregonstate.edu (K. Anderson)*
[b]*Oregon State University-Cascades, 1500 SW Chandler Ave, Bend, OR 97702, USA, email: zhangxi8@oregonstate.edu*

Received 8 June 2022; Accepted 20 September 2022

ABSTRACT

Desalination technologies face fouling challenges (particularly on heat exchanger surfaces) which causes lower heat transfer and freshwater yield. Few studies have focused on multi-salt high salinity solutions (well above seawater) during pool boiling. This study investigates the effect of a heat exchanger's surface roughness on fouling resistance and heat transfer coefficient in a highly saline (20% by mass) pool boiling environment. The average surface roughness was tested at 0.35, 5, and a 10.5 μm (microchannel surface). The 0.35 μm surface had a 1.5 cm^2 K/W lower fouling resistance compared to the other tested surfaces. 5 and 10.5 μm heat exchange surfaces had nearly identical heat transfer performance with fouling resistances of 2.7 cm^2 K/W after 2 h. Decreasing the surface roughness reduced fouling for smooth surfaces (0.35 μm) but had minimal impact on sufficiently rough surfaces (5–10.5 μm). Additional tests determined the effect adding 3% ethylene glycol had on the fouling resistance, heat transfer coefficient, and salt composition for the 10.5 μm surface. Ethylene glycol had no effect on the fouling resistance or heat transfer coefficient; however, it effected the fouling composition. This study will help inform heat exchanger surface design for utilization with high salinity water.

Keywords: Crystallization fouling; Ethylene glycol; Fouling; Saline; Surface roughness

1. Introduction

The demand for water is increasing due to industrialization, higher standards of living, and population growth. Increased demand combined with the depletion of natural freshwater resources has led to water scarcity in many countries around the world. According to the United Nations Water Organization [1], over 2.3 billion people experience high water stress at least one month per year. Desalination technologies present an opportunity to meet the increased demand and eliminate/reduce water scarcity. Many desalination systems use a membrane or thermal based distillation approach. Thermal based approaches commonly evaporate seawater using a heating element and then condense water, leaving salts and other impurities behind.

Fouling, or material surface deposits, is a large problem in desalination technologies. Fouling deposits can lower heat transfer efficiencies, increase pressure drop, and increase corrosion leading to increased maintenance costs in desalination systems [2,3]. The five main fouling types are: biological, corrosion, particulate, chemical, and crystallization fouling. Crystallization, or scale, fouling accounts for 70% of total fouling in desalination systems, as seawater is primarily inorganic [2]. As salts have low thermal conductivity (~0.5–2 W/m·K), fouling build-up reduces the heat transfer coefficient leading to a reduction in the system's overall efficiency. Crystallization fouling is difficult to accurately predict or model as it depends on many parameters including momentum, heat and mass transfer, material

* Corresponding author.

properties, heating configuration, surface temperature, and salt concentration [3–6].

1.1. Salt concentration and types

Crystallization fouling is highly dependent on the degree of supersaturation in a solution as higher salinities have more potentially fouling salts, faster fouling rates, and increased nucleation sites available for crystals growth [3,7]. Increasing calcium chloride concentration was found to increase fouling resistance and shorten the induction time (duration when fouling resistance is greater than nucleation site enhancement) [8]. Many studies have investigated fouling with low salinity solutions (0.0034%–0.4%), but few have studied fouling characteristics in saline solutions higher than 0.4% [3–5,9]. Highly saline brine is often a by-product of desalination and other industrial processes that is often untreated and directly discharged which can degrade soil and ground water [10]. Brine treatment technologies have not been cost effective compared to cheaper, and more environmentally damaging disposal methods [11].To improve high salinity desalination efficiency and extract the maximum amount of water, fouling behavior in highly saline environments needs to be understood and quantified.

Different salts have different adherence, solubility, and heat transfer characteristics. The solubility of different salts impacts the fouling quantity and fouling rate. Salts with decreased solubility at higher temperatures generally begin crystallization fouling [12]. Low salinity calcium sulfate and calcium carbonate fouling has been extensively studied as they have a high fouling resistance (7 cm^2 K/W) and are commonly found on fouled heat exchanger surfaces after 100 h in subcooled boiling conditions [3,4,8,13]. While individual salts have been well studied, there has been limited research on multiple salt mixtures and how their interactions influence fouling behavior.

Helalizadeh et al. [3] studied a mixture of calcium sulfate and calcium carbonate fouling in a subcooled flow boiling system. They showed mixed salts have higher fouling resistance than individual salts in 66% of the concentrations tested and the highest resistance occurred with a mixture of salts [3]. Song et al. [14] compared the fouling resistance of $CaCO_3$ and $CaSO_4$ in different concentrations and found in 75% of the tested cases mixed salt fouling was higher than individual salt fouling. More studies are needed regarding multiple salt solutions as desalination systems rarely treat water with 1–2 salts and the presence of additional salts can change the fouling behaviors.

1.2. Surface roughness effect on fouling

Increased surface roughness impacts both boiling characteristics and fouling accumulation. MacAdam and Parsons [15] found that increasing the average surface roughness (R_a) by 0.6 μm caused an increase in fouling even in a limited (0.2–0.8 μm) surface roughness change. It also increased deposit adhesion-up to 30X more stress is required to remove $CaCO_3$ and $CaSO_4$ fouling from a rough vs. a smooth surface (0.1–21 μm) [6,16]. However, for a smaller change in surface roughness (0.018–0.246 μm), Liu et al. [17] found that smoother surfaces did not show fouling or adhesion reduction for calcium bicarbonate fouling. Fouling adhesion is important as many crystallization fouling resistance curves reach a plateau where the fouling accumulation rate and the removal rate (due to the flow's sheer stress) is equal. Surface roughness manufacturing techniques and geometries should be considered as they could have the same average roughness value but have different fouling impacts [18].

The impact of various roughness values on nucleate boiling have been studied for average surface roughness (R_a) of 0.04–1.5 μm systems [19]. Rougher surfaces have increased phase change heat transfer due to increased agitation from improved bubble formation [19]. Jones et al. [20] studied the effect various surface roughness had on pool boiling heat transfer in pure water and found no additional benefit to increased average surface roughness for 1.08 to 10 μm; but did not consider how it would be affected by fouling. As fouling adheres, the depositions can change the surface roughness of a material, thus impacting other factors that affect fouling accumulation. For example, as salts begin to accumulate in a tube heat exchanger, they increase the surface roughness and restrict the flow volume which increases the friction factor and heat transfer resistance. However, it also increases the shear stress from accelerating the flow [18]. Surface coatings have been one area of interest to reduce fouling as they can change the surface characteristics (roughness, hydrophobicity, etc.). Surface coatings add cost and heat transfer resistance due to the coating material itself. They also degrade over time and only work for specific materials [21,22].

1.3. Boiling effect on fouling

During boiling with crystallization fouling, salt deposits can temporarily increase the heat transfer rate due to increased nucleation sites and near wall turbulence; however, overtime the increase in nucleation sites cannot overcome the fouling resistance and the heat transfer rate decreases [12,18]. Many studies have focused on fouling in subcooled boiling environments, despite evidence showing fouling accumulation is a much larger issue in pool boiling situations due to the bubble formation mechanisms and detachment [3,9,13,23]. Subcooled boiling is common in heat exchangers as boiling only occurs on the heated surface, but the bulk of the fluid is subcooled. Forced convection in subcooled boiling has a significant impact on the rate of fouling accumulation compared to pool boiling [9]. While subcooled boiling and fouling in convective heat transfer have been studied, there is limited information available for mixed salt, high salinity fouling during pool boiling.

Fouling in a pool boiling system occurs due to bubble formation and micro-layer evaporation. Therefore, methods used to increase bubble formation to improve boiling efficiency have a high chance of also increasing crystallization fouling [9]. As bubbles form on the heated surface, the bubble's interface becomes supersaturated which results in salt deposits. Raghupathi and Kandlikar [5] studied pool boiling fouling on a flat heat transfer surface experiment using artificial seawater (0.0034% wt. salt). They found that boiling seawater compared to pure water increases the critical heat flux (CHF) due to increases in nucleation site density from

fouling accumulation. Crystallization fouling also increased thermal resistance and therefore the wall superheat [5]. Jamialahmadi and Müller-Steinhagen [23] compared pure water to a 0.1% salinity calcium sulfate solution during pool boiling. They found bubble departure diameter was increased for saline solutions and the heat transfer coefficient changed based on bubble formation mechanisms. The presence of salt creates a porous layer which can cause the boiling to resemble wick boiling with multiple steam channels through the salt layer [23]. Understanding how surface and pool boiling mechanisms are altered in the presence of a porous salt layer is important to determine how boiling saline water on different surfaces and with higher salinities will impact the overall fouling accumulation and heat transfer.

1.4. Ethylene glycol effect on fouling

To better design evaporators and heat transfer surfaces in desalination units, studies need to be done to understand the impacts of mixed salt saline solutions and various surface roughness' on fouling. It is equally important to understand how the presence of other compounds in a saline solution could affect the fouling resistance and heat transfer coefficient. Several studies have found that a polyethylene glycol (PEG) based coating on a membrane can be used to reduce crystallization and biological fouling in seawater systems [24–26]. PEG is created after ethylene glycol reacts with itself in water creating a variety of ethylene glycol units which are soluble in many organic solvents. PEG is found in many commonly used products [24,27]. While there has been success with creating ethylene glycol-based surface coatings to mitigate fouling in reverse osmosis' processes, these coatings have had minimal use in evaporation-based desalination systems. In addition, ethylene glycol has been used in oil and gas refinement to remove sodium chloride as it is more soluble in ethylene glycol than water [28]. The use of ethylene glycol to remove salts is not common in desalination systems and there is limited information on how ethylene glycol interacts with each salt in a mixed salt solution. Further information is also needed on how ethylene glycol affects fouling, or if it could be applied to systems outside of a reverse osmosis-based desalination system.

A new technology from Oregon State University uses a humidification–dehumidification process to treat hydraulic fracturing wastewater (~20% salinity with other compounds including ~3% ethylene glycol) [29–31]. If ethylene glycol can be separated during desalination, and if it reduces fouling, it could indicate if desalination techniques can be used to treat highly contaminated wastewater. Nikooei et al. [31], using a representative hydraulic fracturing wastewater mixture, found evaporation separated most contaminants including ethylene glycol. There was no mention of how additional solution contaminants effected crystallization fouling, so this question requires further research. This report addresses the effect that ethylene glycol has on crystallization fouling in a highly saline solution (20%).

1.5. Current work

Fouling accumulation changes based on salt, time, flow rate, surface properties, heat and mass transfer, concentration etc. making it difficult to predict. These characteristics have been studied for specific situations with low salinities, subcooled boiling systems, and single salt solutions [3,4,5,9]. Limited information is available for high salinity fouling with more than two mixed salts in pool boiling conditions on various surface roughness'. Understanding how the mentioned conditions effect fouling accumulation could be utilized to effectively treat high salinity solutions that are generally an untreated by-product of desalination. The brine naturally contains multiple salts, and salt mixtures have different fouling characteristics compared to single salt solutions [3]. Estimating the fouling resistance on different heating surfaces during operation is important to track changes to the process efficiency and maintenance costs associated with high salinity mixed salt fouling. The present study focused on determining the heat transfer fouling resistance on a vertical heated surface in a high salinity mixed salt pool boiling environment. This study was designed to isolate the effect of surface roughness on fouling resistance by testing several heating surface roughness values (homogeneous surface roughness' of 0.35, 5 μm, and a heterogeneous surface with microchannels with an average surface roughness of 10.5 μm). The 10.5 μm microchannel surface roughness test was repeated with an additional 3% ethylene glycol in the solution to determine the effect on fouling. Ethylene glycol is used in antifouling coatings and found in many products, but minimal studies have considered the fouling effects when the solution contains ethylene glycol.

2. Experimental setup

Fig. 1 shows the experimental and actual setup used in the current study. A cartridge heater (120 V, 500 W) was embedded into a 115 mm × 50 mm × 50 mm aluminum 6061 block which was submerged in saline water. Aluminum was chosen for the block material as it has a higher fouling accumulation compared to brass and stainless steel. Aluminum surfaces present fouling much quicker and reduce the standard multiple day experiments to a few hours [4,14]. Using aluminum also prevents corrosion issues that would have occurred with ferrous heat exchangers. The cartridge heater was controlled with a Belee 20A variable voltage transformer and the power was measured with a BALDR Power Meter. The heater power was fixed at 200 W and recorded every 30 min throughout each test. The aluminum block had 16 Type K thermocouples embedded 25 mm into the block to measure the block's temperature radially to avoid any temperature bias from hot spots (Fig. 1B). The embedded thermocouples holes were filled with boron nitride thermal paste and sealed with Dowsil RTV sealant to avoid water interacting with the embedded thermocouples. Silicone rubber was also used to secure insulation (Superwool plus MD paper) to the bottom of the block to avoid heat losses to the water through the bottom surface. Additionally, a thermocouple was embedded on the outside the insulation to ensure it was preventing heat loss as intended. During the 2.5-h tests, this measured temperature on the outside of the insulation was below the block temperature. Therefore, the bottom area could be neglected in the fouling resistance analysis as focus was on the radial temperature distribution.

The aluminum block's roughness was adjusted between tests to achieve average R_a values of 0.35, 5, and 10.5 μm measured with a profilometer (Mitutoyo SJ-201) at six different locations on each side of the block. The R_a values from each of the 24 locations (6 × 4) were averaged to get a R_a value for the whole block. Sandpaper was used to achieve the homogeneous 0.35 and 5 μm surface roughness' (Fig. 2). A Dremel was used to cut shallow horizontal and vertical lines in a grid pattern to achieve microchannels with an average surface roughness of 10.5 μm as these are common in boiling systems (Fig. 2).

The saline mixture was continuously mixed using a magnetic stirrer before being pumped into the testing chamber using a Masterflex L/S displacement pump to control the flow rate. At the top of the chamber openings were added for the vapor to escape. The flow rate was adjusted to compensate for the evaporated water and keep the block's surfaces submerged. Two Resistance Temperature Detector (RTDs), used to measure the water temperature, were located on opposite sides of the block 5 mm from the block's surface and 50 mm from the top so that they were in the same horizontal plane as the embedded thermocouples. All thermocouples and RTD temperatures were recorded using an Agilent 34970A DAQ. The power meter, thermocouples, and RTD measurements were used to determine the thermal resistance and heat transfer coefficient due to fouling. After the experiment, the saline water was removed from the excess discharge port. The block's surface, RTDs, and the testing chamber were thoroughly scrubbed with water between tests to remove all salts and ethylene glycol.

The saline water was mixed to match seawater (Sea Salt ASTM D1141-98 [32]) as shown in Table 1 (salts with less than 1% concentration in seawater were neglected). The total salts were scaled to create 20% saline water for tests as shown in Table 2. Using 20% saline water reduced the total test time as fouling occurred more quickly. The 20% saline feed water solution also ensured each test was focused on a heating/evaporating processes that manage brine or other highly saline solutions. A test matrix with operation parameters for all experiments conducted is shown in Table 3.

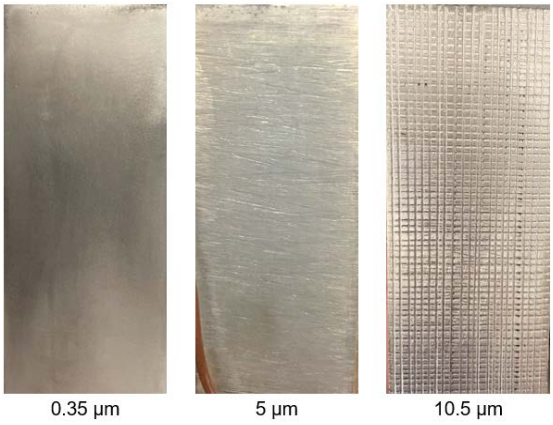

Fig. 2. Aluminum block with different roughness, 0.35 and 5 μm were achieved using sandpaper creating a homogeneous surface roughness, and 10.5 μm was achieved with a Dremel creating microchannels and a heterogeneous surface.

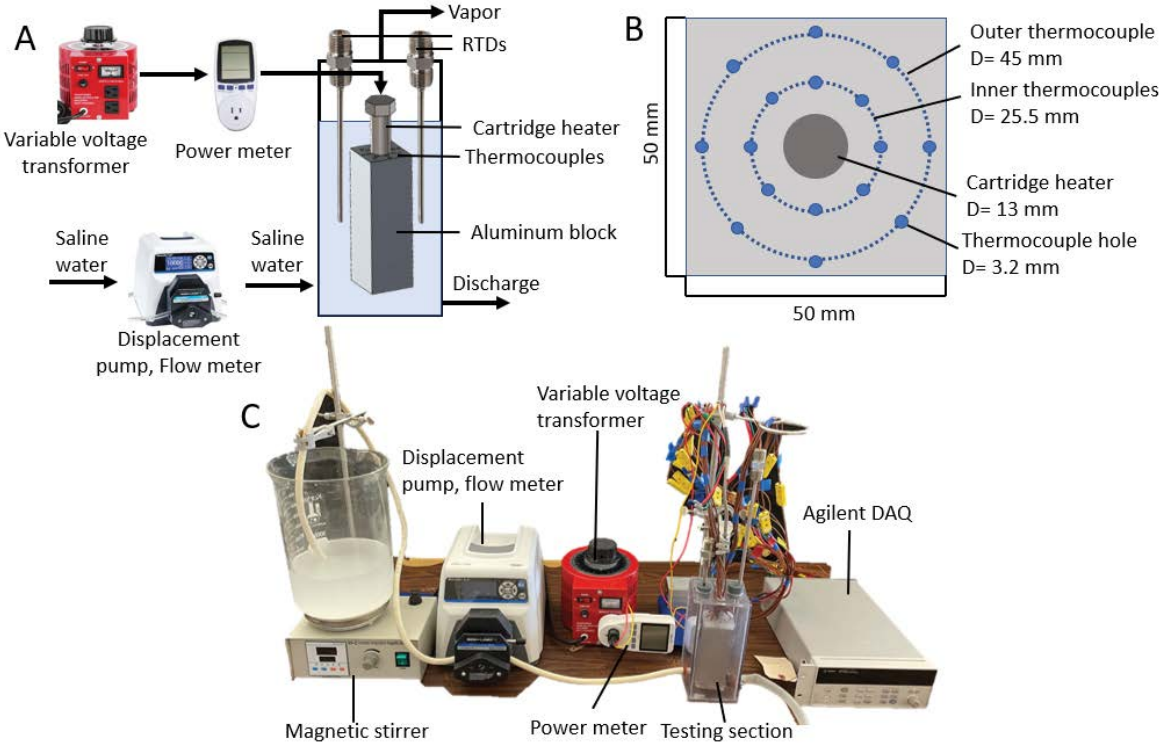

Fig. 1. Experimental set-up used to determine the fouling resistance and the heat transfer coefficient for various surface roughness and solutions (A) experimental schematic, (B) schematic showing the top view of the aluminum block and (C) actual set-up.

Table 1
Salts used in a representative seawater composition (ASTM D1141-98 [31])

Compound	Symbol	Weight percentage
Sodium chloride	NaCl	58.5%
Magnesium chloride	$MgCl_2$–$6H_2O$	26.5%
Sodium sulfate	Na_2SO_4	9.8%
Calcium chloride	$CaCl_2$	2.8%
Potassium chloride	KCl	1.6%
Other salts	–	0.8%

Table 2
Testing solution for experiments with and without ethylene glycol

Compound	Brine 1 (no ethylene glycol) (wt.%)	Brine 2 (with ethylene glycol) (wt.%)
Water	80.1%	77.8%
Sodium chloride	11.7%	11.4%
Magnesium chloride	5.3%	5.2%
Sodium sulfate	2%	1.9%
Calcium chloride	0.6%	0.5%
Potassium chloride	0.3%	0.3%
Ethylene glycol	0	2.9%

Table 3
Surface roughness crystallization fouling experimental test matrix

Experiment number	Salinity (wt.%)	Ethylene glycol (wt.%)	Average aluminum surface roughness (μm)
1	20	0	0.35
2	20	0	5
3	20	0	10.5
4	20	3	10.5

Each experiment in Table 3 was conducted 3 times to ensure repeatability for a total of 12 tests.

To determine which salts attributed to the crystallization fouling, the attached salts were removed from the aluminum block by dissolving the crystalized salts in distilled water. Once all salts had been dissolved into the water, the water was evaporated leaving behind only the salts that had attributed to the crystallization fouling. The accumulated salts from the tests with and without 3% ethylene glycol in the solution were analyzed using inductively coupled plasma-optical emission spectrometry (ICP-OES) with nitric acid as the dilutant (inductively coupled plasma-optical emission spectrometry) to quantify composition.

3. Methodology

The methodology used to analyze the data is consistent with literature [3,8,10,13]. To determine the fouling resistance, R_f, between the heat exchange surface and the saline water solution, Eq. (1) was used.

$$R_f = \frac{1}{h_f} - \frac{1}{h_o} \tag{1}$$

where h_f is the heat transfer coefficient between the heat exchange surface and boiling water as fouling occurs, and h_o is the initial heat transfer coefficient at the beginning of the test. h_f and h_o are calculated using Eqs. (2) and (3) where q'' is the heat flux produced by the heater. q'' was assumed to be uniform throughout the block. $T_{s,f}$ and $T_{w,f}$ are the surface temperatures of the heat exchange surface and the water, respectively, as fouling occurs. $T_{s,o}$ and $T_{w,o}$ are the temperatures of the heat exchange surface and the water at the beginning of the test before any fouling has occurred. To provide a clear comparison between tests, all h_o values were reference when $T_{w,o}$ = 101°C.

$$h_f = \frac{q''}{T_{s,f} - T_{w,f}} \tag{2}$$

$$h_o = \frac{q''}{T_{s,o} - T_{w,o}} \tag{3}$$

The heat flux, q'', is calculated by dividing the measured heater power, read from the digital power meter, by the surface area of the aluminum block that was in contact with the saline water. The heat transfer surface area only included the sides of the block as the top and bottom of the block were insulated forcing all the heat to exit through the sides of the block. Both water temperatures, $T_{w,o}$ and $T_{w,f}$, were measured as the average of the two RTDs that were submerged roughly 50 mm under the surface of the boiling water. The surface temperatures of the block, $T_{s,o}$ and $T_{s,f}$, were calculated using the average of the corner and middle thermocouple measurements for each side. Each average side temperature was then averaged again over all four surface to calculate the average surface temperature for the whole block. The block's surface temperature was calculated using Eq. (4) based on the outer most thermocouple temperature and the measured heat flux.

$$T_S = T_{\mathrm{TC},o} - q'' \cdot R_{\mathrm{al},o} \tag{4}$$

where q'' is the heat flux provided by the heater, $T_{\mathrm{TC},o}$ is the outer ring thermocouple reading, and $R_{\mathrm{al},o}$ is the thermal resistance between the outer thermocouple and the surface of the block. $R_{\mathrm{al},o}$ is calculated using Eq. (5).

$$R_{\mathrm{al,o}} = \frac{D_{\mathrm{al,o}}}{k_{\mathrm{al}}} + \frac{D_{\mathrm{tp}}}{k_{\mathrm{tp}}} \tag{5}$$

where $D_{\mathrm{al},o}$ is the thickness of aluminum in between the edge of the outer thermocouple hole and the edge of the block, D_{tp} is the radius of the hole that the thermocouple was

inserted into (filled with thermal paste), and k_{al} and k_{tp} are the thermal conductivities of aluminum and the thermal paste used to fill the thermocouple holes respectively.

To ensure that the power meter measurements were accurate, the heat flux, q'', was also calculated by an alternative method. Using the temperature difference between each set of the inner and outer thermocouples ($T_{TC,i}$ and $T_{TC,o}$ respectively), and the thermal resistance between each set of thermocouples, $R_{al,i}$, q'' was calculated as shown in Eq. (6).

$$q'' = \frac{T_{TC,i} - T_{TC,o}}{R_{al,i}} \tag{6}$$

Next, each of the q'' values calculated from the thermocouple temperatures were compared to the q'' values measured from the power meter. These two methods of measuring the heat flux produced results that matched within the uncertainty associated with the temperature measurements. As the heat flux values measured from each method produced matching results, the power meter's readings were used to determine the fouling resistance.

3.1. Simulation results

To validate the uniform heat flux assumption, the measured thermocouple values were compared to simulated values calculated by a SOLIDWORKS simulation that assumed a uniform heat flux from the heater's surface. The thermal finite element analysis (FEA) simulation used the water temperature (measured by the RTDs) and the power (measured by the power meter) to calculate the steady state radial heat distribution with no fouling. Fig. 3 shows the steady state temperature distribution across a cross-section of the aluminum block for a uniform heat flux boundary condition applied to the cartridge heater-block interface, and a constant temperature boundary condition applied to the outer heat transfer surface that was in contact with the boiling saline solution. These boundary conditions applied to the cross section of the aluminum block yielded a small temperature distribution (~4°C) across the block. The white dots on Fig. 3 represent the location where the SOLIDWORKS temperature solutions were compared to the actual thermocouple measurement from the experimental data. The simulation matched the measured 16 thermocouple readings within 2%–4%, thus validating the uniform heat flux assumption used to calculate the fouling resistance and heat transfer coefficient. In addition, there is minimal temperature difference between the sides and corners of the block in the simulation however the corner temperatures during the experiment were still calculated and averaged for each side using the discussed methodology.

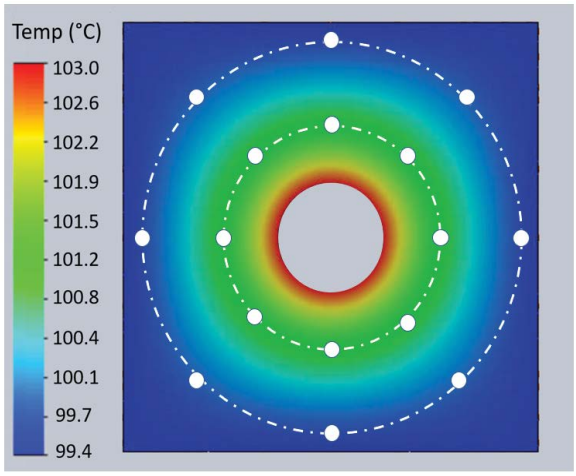

Fig. 3. SOLIDWORKS simulation showing radial temperature distribution for q'' = 66,000 W/m^2 and 97.4°C water temperature. 2%–4% error compared to measured thermocouple data.

A mesh independence study was conducted for mesh sizes between 0.5–2 mm and found a change in error between the simulated and experiential temperatures to be very low (0.03%–0.66%). To reduce computational power and maintain adequate accuracy, a mesh size of 0.75 mm was used to simulate the temperatures with a uniform heat flux.

3.2. Uncertainty propagation

The RTDs were calibrated by recording the reference resistance, R_0, during an ice bath, and then averaging this reference resistance over 3 separate ice bath tests. Using the average reference resistance value form the ice bath tests, the temperature was calculated using Eq. (7) by applying the A and B coefficients provided by the RTD manufacturer. After calibration, the RTD uncertainty was determined to be ±0.125°C. Type K thermocouples were calibrated by comparing the calibrated RTD temperatures to the thermocouple readings in both an ice bath and a hot water bath. This was done to account for any offsets in the thermocouple readings. After calibration, all the type K thermocouples showed an uncertainty of ±0.5°C. If any of the 16 thermocouples failed (readings were not read properly by the DAQ) during the test, an average of the two adjacent thermocouples was taken as there were minimal differences in temperature measurements along the same radius.

$$R(T) = R_0\left(1 + A \cdot T + B \cdot T^2\right) \tag{7}$$

The uncertainty from each of the measured values was propagated to the final fouling resistance value using the Kline-McClintock method implemented in Engineering Equation Solver (EES) [33]. The uncertainties included both measurement and precision uncertainty. As boiling is random in nature, many of the temperature measurements during the middle of the test had high variation between the 3 repeated tests. As the overall temperature change, and by extension, fouling resistance over the course of the entire test was the most substantial finding from this work, only the average temperatures of the first and last 5 min of each test were used to calculate the precision uncertainty associated with the repeated tests. Quantization uncertainty associated with the DAQ sampling rate was calculated for each sensor, but they were found to be insignificant compared to the other uncertainties. The final uncertainty values for all measured and calculated values are shown in Table 4.

Table 4
Uncertainty values for all measured values used in data analysis

Parameters	Uncertainty		
	Minimum	Average	Maximum
Thermocouple (°C)	–	0.5	–
RTD (°C)	–	0.1	–
Heater power (W)	–	3.5	–
Fouling resistance (cm^2 K/W)/%	0.440/11.7	0.503/23.9	0.607/60.7
Heat transfer coefficient (W/cm^2·K)/%	0.008/3.2	0.019/9.8	0.046/17.7

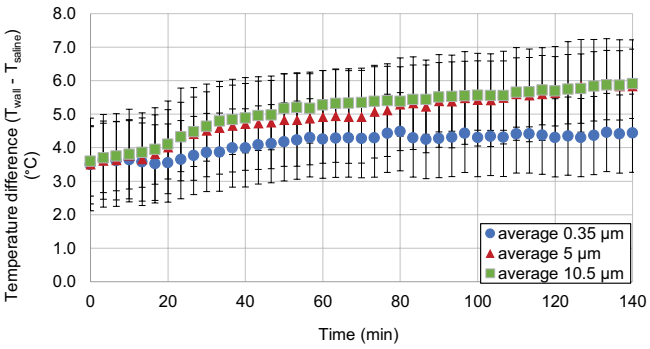

Fig. 4. Impact of surface roughness on temperature difference. Temperature difference is due to increased wall temperature which indicates increased resistance due to fouling accumulation over time.

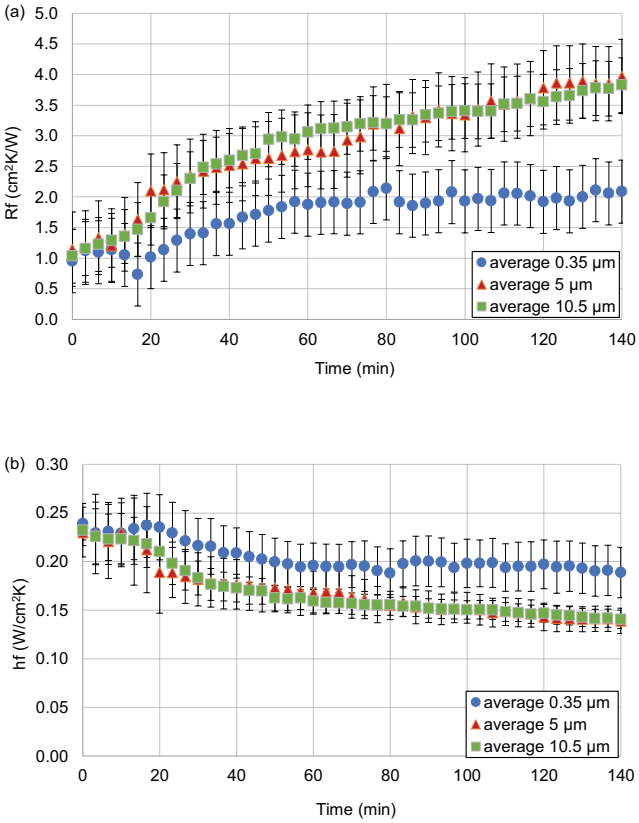

Fig. 5. (A) Impact of surface roughness on fouling resistance. 0.35 µm test has asymptotic fouling rates after 60 min with the lowest fouling resistance. The 5 and 10.5 tests have stronger fouling adhesion and nearly identical linear fouling resistance, and the fouling layer will continue to grow with time. (B) Impact of surface roughness on heat transfer coefficient. During the first 20 min it shows an initialization period where there is limited impact on the heat transfer coefficient due to fouling accumulation before it degrades in all instances.

4. Results and discussion

4.1. Temperature difference

Fig. 4 shows the difference between the wall temperature and the water temperature during the experiment. As the water temperature is consistent during the test, the change in the temperature difference is due to an increase in wall temperature from fouling accumulation decreasing heat transfer. The temperature difference between the 5 and 10.5 µm microchannel is very minimal meaning the wall temperature increase was the same and thus likely the same fouling accumulation occurred between tests. The 0.35 µm test had a much lower change in temperature indicating minimal fouling accumulation occurred. This is important as the temperature difference was used to calculate the heat transfer coefficient and fouling resistance. This makes the temperature difference a good indicator of fouling accumulation and resistance present on the heater surface.

4.2. Effect of surface roughness on fouling

Fig. 5A shows the effect of surface roughness on both the fouling resistance and the heat transfer coefficient. The trend for all tests is consistent with literature as there is an initialization (induction) period that occurs at the beginning of testing where fouling increases the surface roughness. In some cases, this initialization period can have a positive impact on the heat transfer coefficient due to increased surface roughness before fouling begins to dominate [3,9,12]. In this study, the initialization period occurs in the first 20 min and has minimal effect on the heat transfer coefficient as this period is happening very quickly due to the high salinity. As show in Fig. 5B, the 0.35 µm test's heat transfer coefficient increases and the fouling resistance decreases in the first 20 min. This is due to the increased nucleation sites and increased surface roughness with small traces of fouling that leads to increased boiling. After this initialization period (first 20 min of testing) the fouling resistance dominates over the increase in nucleation sites as more salts accumulate on the surface. The graph in Fig. 5B also shows a linearly increasing trend for both the 5 and 10.5 µm (microchannel) tests throughout 140 min indicating the fouling has strong adhesion and the fouling removal rate (due to boiling stress) is lower than the fouling accumulation rate. The 0.35 µm test has an increasing trend for the first 60 min before plateauing indicating that fouling is asymptotic meaning that the increase in deposits and the removal of deposits from the shear stress of boiling occurring is equal and the deposits

are weaker compared to other cases. This also indicates that a constant fouling resistance of 2 cm² K/W would be a good estimate for a system with a heating surface of 0.35 μm roughness, whereas a constant value for the 5 μm or the 10.5 μm test would be inaccurate for modeling operations as the fouling resistance increases with time and is not constant.

In Fig. 5A, the fouling resistance for the 0.35 μm surface increases about 1 cm² K/W in 120 min while the 5 and 10.5 μm surface roughness increases the resistance by ~2.7 cm² K/W. The 5 μm homogeneous surface roughness and 10.5 μm microchannel surface roughness had nearly identical values and trends for the heat transfer coefficient and fouling resistance. Indicating that the additional surface roughness from the addition of microchannels in the 10.5 μm microchannel test had no impact on the fouling accumulation. There is also no benefit from reducing a heater's surface from 10.5 μm with microchannels to a homogeneous surface roughness of 5 μm, but there is a benefit when reducing the surface roughness from 5 to 0.35 μm. With surface roughness' larger than 10.5 μm, it would be expected to see fouling accumulation increase with surface roughness as the number and size of the nucleation sites changes and surface roughness becomes a more dominant indicator of fouling. Reducing the average surface roughness can decrease the affect surface roughness has on fouling accumulation if it is sufficiently reduced (5 to 0.35 μm) but reducing the surface roughness does not mitigate fouling when the surface is sufficiently rough.

Fig. 5B shows the effect of surface roughness on the heat transfer coefficient. All three tests have very similar trends and values for the heat transfer coefficient indicating that the surface roughness has only a small impact on this value. The heat transfer coefficient mirrors the fouling resistance values in that they plateau after 60 min indicating the heat transfer coefficient is constant after sufficient fouling has occurred. The 5 and 10.5 μm tests had slightly lower (~0.05 W/cm²·K) heat transfer coefficients even initially when minimal fouling was occurring. This is counter intuitive as generally the rougher the surface for non-fouling pool boiling leads to higher heat transfer coefficients due to increased nucleation sites, increased turbulence, and lower fouling [6,18,34]. One reason for this discrepancy could be because the adhesion strength at rougher surfaces is higher, requiring more stress to remove fouling, and therefore the fouling layer is thicker as seen in Fig. 5A leading to a lower heat transfer coefficient for the homogeneous 5 and 10.5 μm microchannel tests.

4.3. Effect of ethylene glycol on fouling

After all surface roughness tests were completed, the heterogeneous 10.5 μm surface with microchannels tests was repeated with an additional 3% ethylene glycol (EG) by mass to determine if an organic compound would influence the fouling resistance or heat transfer coefficient. EG was chosen as it is used in many anti-fouling surface coatings and used in the gas industry to remove sodium salts. Fig. 6 shows the fouling resistance and heat transfer coefficient results discussed previously with the addition of the

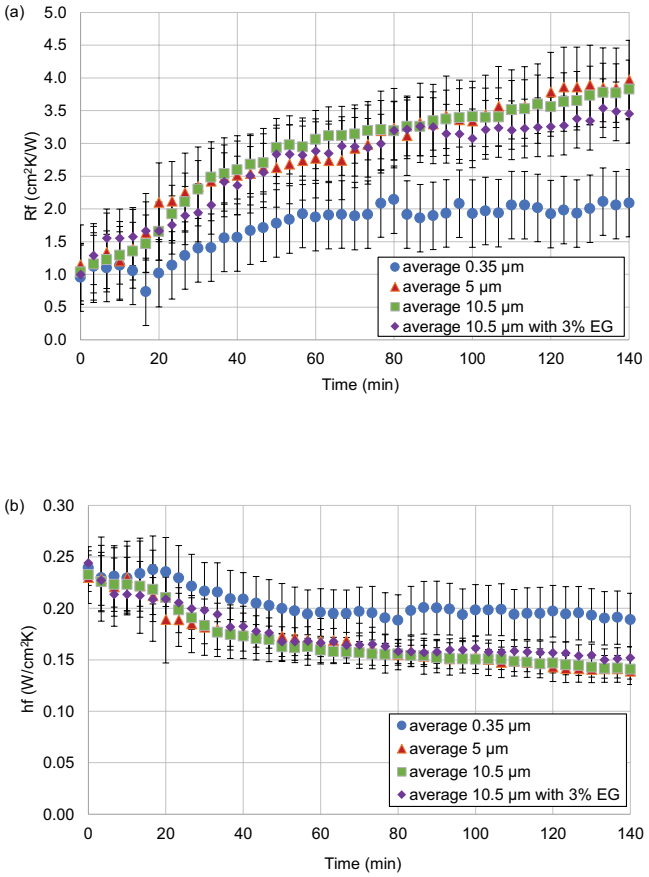

Fig. 6. (A) Impact of surface roughness and ethylene glycol (EG) on fouling resistance. The addition of 3% EG has the same effect on fouling resistance as the 5 and 10.5 μm without the EG's presence in the solution. (B) Impact of surface roughness and ethylene glycol (EG) on heat transfer coefficient. The addition of 3% EG has the same effect and trend on the heat transfer coefficient as the 5 and 10.5 μm without the EG's presence in the solution.

test with 10.5 μm microchannel surface roughness with 3% EG included in the solution. The test with ethylene glycol had no identifiable effect on the fouling resistance or heat transfer coefficient compared to the 10.5 μm test with saline water. Therefore, adding ethylene glycol to a high salinity solution does not affect the overall fouling resistance.

Fig. 7 shows example pictures of the aluminum surface after a 140-min test for the 3 surface roughness conditions and the test with 3% EG. These pictures further emphasize that the homogeneous 0.35 μm surface had less fouling accumulation than the other tests as it has the least amount of visible fouling and un-fouled surfaces can be seen. In the 0.35 μm picture, at the top of the aluminum there is a section which is completely fouled which corresponds with the water level during the test. This indicates that the water-steam interface may have a high impact on fouling accumulation as the liquid vaper interface has the fastest rate of salts separating and thus results in the highest quantity of fouling deposits. In the 5 and 10.5 μm pictures the surface is covered with salt accumulation and there is minimal difference between the fouling coverage. These pictures

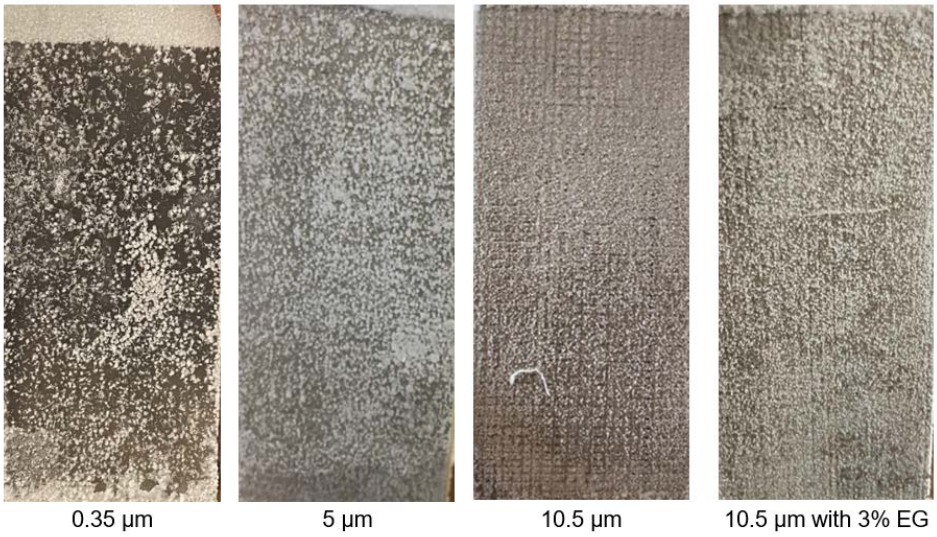

Fig. 7. Example pictures of crystallization fouling for 0.35, 5, 10.5, and 10.5 µm with 3% ethylene glycol in the solution after 140 min where the 0.35 µm test has the least amount of fouling coverage on the block, the 5 and 10.5 µm test's have similar fouling distributions. There are different visual crystal structures present between the 10.5 µm tests with and without 3% EG present.

are consistent with the measured data for both the fouling resistance and heat transfer coefficient.

In the 10.5 µm microchannel tests with and without the EG, the fouling has begun to fill and cover the grooves that were on the surface, changing the surface roughness as more salt accumulates and reducing the impact of the microchannels used in boiling systems. Comparing the 10.5 µm pictures, with and without EG in the solution, it is apparent that the crystal structure is different between the two tests, and that the test with EG in the solution has more coverage. This is important as the overall effect of fouling was the same despite the visual differences indicating that the accumulated salts may have changed.

3% EG was chosen for this work as it is estimated to be present in hydraulic fracturing wastewater and, if used in a desalination system, would need to be separated. Understanding the impact of EG on fouling will change the required operation and maintenance of purifying hydraulic fracturing [29]. While this data shows no change in the fouling resistance or heat transfer coefficient as a result of the added EG further research should be done to understand if other organic compounds have an impact on fouling and if so, what salts are affected. Understanding how fouling reacts with different chemicals present within the solution will help expand what mixtures can be treated using common desalination technologies.

4.4. Effect of EG presence on salt composition

While there was no difference in the measured fouling resistance values with and without the presence of ethylene glycol in the solution, the salts that adhered to the surface did appear to be a different structure. Therefore, the adhered salts were removed from the block and tested using ICP-OES analysis to determine the composition of fouled salts. Fig. 8 shows the different elements that accumulated on the heat exchange surface with and without the

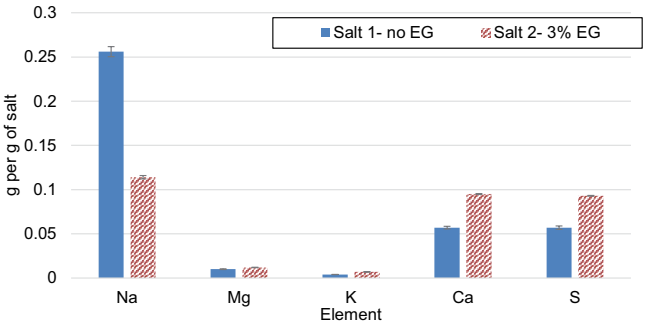

Fig. 8. ICP-OES data showing the elements that accumulated on the aluminum block's surface for a 10.5 µm surface roughness with (salt 2) and without (salt 1) 3% ethylene glycol (EG) present in the solution. The addition of EG in the solution changes which salts are contributing to fouling as the number of sodium ions greatly decreases and the amount of calcium and sulfur ions increase.

3% EG in the solution. Magnesium, potassium, calcium, and sulfur elements can each be attributed to one salt dissociating (magnesium chloride, sodium sulfate, calcium chloride, and potassium chloride, respectively), however the sodium elements could come from either the sodium chloride or the sodium sulfate as both have sodium ions. With no EG present, there is significantly more sodium ions that contributed to fouling than with 3% EG, however with the 3% EG there is an increase in calcium and sulfate ions. Some decrease in sodium ions was expected as sodium chloride is 22.6% more soluble in ethylene glycol than in water at 20°C, however the sodium ions reduced by 44.6% for only adding 3% EG indicating that the addition of other salts also affected the solubility and fouling composition [28]. The addition of EG increased the number of calcium and sulfate ions that fouled indicating their solubility and probability of fouling was strongly affected as well. Despite a

large percentage of magnesium chloride in the original solution (26.5% of initial salts), only very small amounts of magnesium and potassium ions contributed to fouling with or without the presence of 3% EG indicating they are unlikely to cause large fouling problems in a boiling system.

While there was no change in the overall fouling resistance with or without EG present, it has only affected which salts are attributing to crystallization fouling. In tests with and without EG, sodium ions were the largest attributers to crystallization fouling. This suggests that salts with sodium ions must be carefully managed to avoid fouling accumulation. Therefore, adding EG into a solution could be useful to reduce specific salts from fouling such as those containing sodium ions if those specific salts have higher adhesion or unattractive qualities. Further research should be done to understand how concentration and type of organic compound affects the salts that adhere to heat exchange surfaces and if any compounds could reduce the effect of fouling.

5. Conclusion

Prior to this study, fouling characteristics had been studied for specific situations such as low salinities (that of seawater or less), subcooled boiling systems, and single salt solutions. This study adds to existing literature by determining the fouling resistance and heat transfer coefficient as mixed salts accumulate on a heat exchange surface with different surface roughness in a high salinity pool boiling environment. This study determined the effect of fouling on 0.35, 5, 10.5 μm surface roughness with a 20% salinity solution made up of most prevalent five salts found in natural seawater (sodium chloride, magnesium chloride, sodium sulfate, calcium chloride, potassium chloride) to mimic desalination brine discharge.

This study found fouling resistance does not increase as surface roughness increases from 5–10.5 μm. However lowering the surface roughness to 0.35 μm does decrease the fouling resistance by 1.5 ± 0.5 cm^2/W. In addition, the fouling resistance associated with 5 and 10.5 μm surface roughness increases linearly for after the initialization period indicating the fouling has strong adhesion to the surface. Whereas the 0.35 μm surface roughness has an asymptotic fouling trend after the first 60 min of the 140 min test indicating a constant fouling resistance value can be used to model the heating surface with 0.35 μm surface roughness. Lastly, this study found there was no change in fouling resistance or heat transfer coefficient in tests with and without 3% ethylene glycol present in the solution. However, the fouled salt's composition did change with the presence of ethylene glycol as sodium based salts were reduced and sulfur and calcium salts increased in the fouling deposits.

Further research is needed to better understand how geometry affects fouling accumulation, and indicates the importance of testing fouling accumulation, determine what dominates fouling when surface roughness is sufficiently smooth (<0.35 μm), and composition with various organic compounds present. The authors are currently working on extensive boiling flow tests with the same mixture of salts to compare the effect of flow and orientation on fouling which will be presented in a future publication. This study also serves to help design heat exchangers in desalination, pharmaceutical, and other industrial applications. A very important application is continental and geothermal brine concentration to extract valuable metals such as lithium or magnesium. Currently, most systems use very large brine pools. This study helps understand the fouling management in assisted pool heating systems for brine concentration or treatment.

Declaration of competing interest

The authors declare that they have no known competing financial interests or personal relationships that could have appeared to influence the work reported in this paper.

Acknowledgements

This work is supported by the US Department of Energy, Advanced Research Projects Agency – Energy (ARPA-E) award number DE-AR-0001000. Results of this work do not necessarily reflect the views of the Department of Energy. The authors acknowledge the support from Kathy Hu and Elnaz Nikooei at Oregon State University in Corvallis, OR for their contributions in experimental design and analysis.

Author contributions

M.M., K.A., X.Z., and B.A. conceived and designed the study. M.M. and K.A. prepared the experimental setup and conducted experiments including collecting and processing data. M.M., K.A., and B.A formulated the paper. All authors analyzed data, approved the final version of the manuscript, and agree to be held accountable for content therein.

Symbols

R_a	—	Arithmetic average of roughness profile
R_f	—	Fouling resistance
h_f	—	Heat transfer coefficient after fouling
h_o	—	Initial heat transfer coefficient
q''	—	Heat flux
$T_{s,f}$	—	Temperature of surface after fouling
$T_{s,o}$	—	Initial temperature of surface
$T_{w,f}$	—	Temperature of water after fouling
$T_{w,o}$	—	Initial temperature of water
T_s	—	Block surface temperature
$T_{\mathrm{TC},o}$	—	Outer thermocouple temperature
$T_{\mathrm{TC},i}$	—	Inner thermocouple temperature
$R_{\mathrm{al},o}$	—	Outer aluminum thermal resistance
$R_{\mathrm{al},i}$	—	Inner aluminum thermal resistance
$D_{\mathrm{al},o}$	—	Outer thermocouple to block surface length
D_{tp}	—	Thermal paste length
k_{al}	—	Thermal conductivity of aluminum
k_{tp}	—	Thermal conductivity of thermal paste
R_0	—	Reference resistance of RTD
$R(T)$	—	Resistance measured by RTD
T	—	Temperature measured by RTD
A	—	A coefficient in Callendar-Van Dusen equation
B	—	B coefficient in Callendar-Van Dusen equation

References

[1] United Nations, Summary Progress Update 2021: SDG 6 — Water and Sanitation For All, 24 February 2021. Available at: https://www.unwater.org/water-facts/scarcity/ (December 2021).

[2] D. Rubio, C. López-Galindo, J.F. Casanueva, E. Nebot, Monitoring and assessment of an industrial antifouling treatment. Seasonal effects and influence of water velocity in an open once-through seawater cooling system, Appl. Therm. Eng., 67 (2014) 378–387.

[3] A. Helalizadeh, H. Müller-Steinhagen, M. Jamialahmadi, Mixed salt crystallization fouling, Chem. Eng. Process. Process Intensif., 39 (2000) 29–43.

[4] S.N. Kazi, K.H. Teng, M.S. Zakaria, E. Sadeghinezhad, M.A. Bakar, Study of mineral fouling mitigation on heat exchanger surface, Desalination, 367 (2015) 248–254.

[5] P.A. Raghupathi, S.G. Kandlikar, Characterization of pool boiling of seawater and regulation of crystallization fouling by physical aberration, Heat Transfer Eng., Selected Papers from the 13th International Conference on Nanochannels, Microchannels and Minichanles, July 6–9, 2015, San Francisco, California, USA, 38 (2017) 1296–1304.

[6] S.N. Kazi, Fouling and Fouling Mitigation on Heat Exchanger Surfaces, J. Mitrovic, Ed., Heat Exchangers, InTechOpen, 2012.

[7] M. Jamialahmadi, H. Müller-Steinhagen, Crystallization of calcium sulfate dihydrate from phosphoric acid, Dev. Chem. Eng. Miner. Process., 8 (2000) 587–604.

[8] A. Janzen, E.Y. Kenig, Analysis of crystallization fouling in electric water heating, Heliyon, 5 (2019) e02695, doi: 10.1016/j.heliyon.2019.e02695.

[9] A. Helalizadeh, H. Müller-Steinhagen, M. Jamialahmadi, Mathematical modelling of mixed salt precipitation during convective heat transfer and sub-cooled flow boiling, Chem. Eng. Sci., 60 (2005) 5078–5088.

[10] A. Panagopoulos, Study and evaluation of the characteristics of saline wastewater (brine) produced by desalination and industrial plants, Environ. Sci. Pollut. Res., 29 (2021) 23736–23749.

[11] A. Panagopoulos, K.-J. Haralambous, M. Loizidou, Desalination brine disposal methods and treatment technologies - a review, Sci. Total Environ., 693 (2019) 133545, doi: 10.1016/j.scitotenv.2019.07.351.

[12] A. Janzen, E. Kenig, Understanding and analysis of fouling behavior or bare-wire heating elements in electric water heating, Heat Exch. Fouling Cleaning, (2019) 1–8.

[13] S.M. Peyghambarzadeh, A. Vatani, M. Jamialahmadi, Application of asymptotic model for the prediction of fouling rate of calcium sulfate under subcooled flow boiling, Appl. Therm. Eng., 39 (2012) 105–113.

[14] K. Sub Song, J. Lim, S. Yun, D. Kim, Y. Kim, Composite fouling characteristics of $CaCO_3$ and $CaSO_4$ in plate heat exchangers at various operating and geometric conditions, Int. J. Heat Mass Transfer, 136 (2019) 555–562.

[15] J. MacAdam, S.A. Parsons, Calcium carbonate scale formation and control, Rev. Environ. Sci. Biotechnol., 3 (2004) 159–169.

[16] S. Keysar, R. Semiat, D. Hasson, J. Yahalom, Effect of surface roughness on the morphology of calcite crystallizing on mild steel, J. Colloid Interface Sci., 162 (1994) 311–319.

[17] Y. Liu, Y. Zou, L. Zhao, W. Liu, L. Cheng, Investigation of adhesion of $CaCO_3$ crystalline fouling on stainless steel surfaces with different roughness, Int. Commun. Heat Mass Transfer, 38 (2011) 730–733.

[18] F. Albert, W. Augustin, S. Scholl, Roughness and constriction effects on heat transfer in crystallization fouling, Chem. Eng. Sci., 66 (2010) 499–509.

[19] J.S. Kim, A. Girard, S. Jun, J. Lee, S.M. You, Effect of surface roughness on pool boiling heat transfer of water on hydrophobic surfaces, Int. J. Heat Mass Transfer, 118 (2018) 802–811.

[20] B.J. Jones, J.P. McHale, S.V. Garimella, The influence of surface roughness on nucleate pool boiling heat transfer, J. Heat Transfer, 131 (2009) 121009, doi: 10.1115/1.3220144.

[21] A. Warlo, B. Nienborg, H. Fugmann, M. Altenberend, L. Schnabel, K. Conzelmann, M. Mathieu, A. Schwärzler, Experimental characterization of fouling in context of heat exchanger development, Heat Exch. Fouling Cleaning, (2019) 1–7.

[22] J.S. Kim, A. Girard, S. Jun, J. Lee, S.M. You, Effect of surface roughness on pool boiling heat transfer of water on hydrophobic surfaces, Int. J. Heat Mass Transfer, 118 (2018) 802–811.

[23] M. Jamialahmadi, H. Müller-Steinhagen, A new model for the effect of calcium sulfate scale formation on pool boiling heat transfer, J. Heat Transfer, 126 (2004) 507–517.

[24] T. Ekblad, G. Bergström, T. Ederth, S.L. Conlan, R. Mutton, A.S. Clare, S. Wang, Y. Liu, Q. Zhao, F. D'Souza, G.T. Donnelly, P.R. Willemsen, M.E. Pettitt, M.E. Callow, J.A. Callow, B. Liedberg, Poly(ethylene glycol)-containing hydrogel surfaces for antifouling applications in marine and freshwater environments, Biomacromolecules, 9 (2008) 2775–2783.

[25] I. Banerjee, R.C. Pangule, R.S. Kane, Antifouling coatings: recent developments in the design of surfaces that prevent fouling by proteins, bacteria, and marine organisms, Adv. Mater., 23 (2010) 690–718.

[26] E.M. Van Wagner, A.C. Sagle, M.M. Sharma, Y.-H. La, B.D. Freeman, Surface modification of commercial polyamide desalination membranes using poly(ethylene glycol) diglycidyl ether to enhance membrane fouling resistance, J. Membr. Sci., 367 (2011) 273–287.

[27] A.L. Truschel, What Is Polyethylene Glycol?, Sciencing, April 2017. Available at: https://sciencing.com/polyethylene-glycol-2507.html (December 2021).

[28] Z. Lu, J. Jiang, M. Ren, J. Xu, J. Da, F. Cao, The study on removing the salts in crude oil via ethylene glycol extraction, Energy Fuels, 29 (2015) 355–360.

[29] B. Abbasi, X. Zhang, H. O'Hern, E. Nikooei, Method and System for Purifying Contaminated Water, United States Patent 62882970, 4 August 2020.

[30] H. O'Hern, E. Nikooei, X. Zhang, C. Hagen, N. AuYeung, D. Tew, B. Abbasi, Reducing the water intensity of hydraulic fracturing: a review of treatment technologies, Desal. Water Treat., 221 (2021) 121–138.

[31] E. Nikooei, N. AuYeung, X. Zhang, K. Goulas, B. Abbasi, A. Dyall, B. Abbasi, Controlled dehumidification to extract clean water from a multicomponent gaseous mixture of organic contaminants, J. Water Process Eng., 43 (2021) 102229, doi: 10.1016/j.jwpe.2021.102229.

[32] ASTM Synthetic Seawater, Sea Salt ASTM D1141-98, Available at: https://www.syntheticseawater.com/products/sea-salt-astm-d1141-98 (December 2021).

[33] H.W. Coleman, W. Glenn Steele, Engineering application of experimental uncertainty analysis, AIAA J., 33 (1995) 1888–1896.

[34] M. Haghshenasfard, G.H. Yeoh, M. Dahari, K. Hooman, On numerical study of calcium sulfate fouling under sub-cooled flow boiling conditions, Appl. Therm. Eng., 81 (2015) 18–27.